Molecular Microbiology (2007) **64**(4), 938–952 doi:10.1111/j.1365-2958.2007.05720.x

The tubulin homologue FtsZ contributes to cell elongation by guiding cell wall precursor synthesis in *Caulobacter crescentus*

Michelle Aaron,[1,2] Godefroid Charbon,[1] Hubert Lam,[1†] Heinz Schwarz,[3] Waldemar Vollmer[4*‡] and Christine Jacobs-Wagner[1*]

[1]*Department of Molecular, Cellular, and Developmental Biology, Yale University, New Haven, CT 06520, USA.*
[2]*Microbiology Program, Yale University, New Haven, CT 06536, USA.*
[3]*Max-Planck-Institut für Entwicklungsbiologie, 72076 Tübingen, Germany.*
[4]*Mikrobielle Genetik, Universität Tübingen, 72076 Tübingen, Germany.*

Summary

The tubulin homologue FtsZ is well known for its essential function in bacterial cell division. Here, we show that in *Caulobacter crescentus*, FtsZ also plays a major role in cell elongation by spatially regulating the location of MurG, which produces the essential lipid II peptidoglycan cell wall precursor. The early assembly of FtsZ into a highly mobile ring-like structure during cell elongation is quickly followed by the recruitment of MurG and a major redirection of peptidoglycan precursor synthesis to the midcell region. These FtsZ-dependent events occur well before cell constriction and contribute to cell elongation. In the absence of FtsZ, MurG fails to accumulate near midcell and cell elongation proceeds unperturbed in appearance by insertion of peptidoglycan material along the entire sidewalls. Evidence suggests that bacteria use both a FtsZ-independent and a FtsZ-dependent mode of peptidoglycan synthesis to elongate, the importance of each mode depending on the timing of FtsZ assembly during elongation.

Accepted 26 March, 2007. *For correspondence. E-mail chistine.jacobs-wagner@yale.edu; Tel. (+1) 203 432 5170; Fax (+1) 203 432 6161; E-mail W.Vollmer@ncl.ac.uk; Tel. (+44) 191 222 6295; Fax (+44) 191 222 7424. Present addresses: †Department of Medicine, Brigham and Women's Hospital/Harvard Medical School, Boston, MA 02115, USA; ‡Institute for Cell and Molecular Biosciences, University of Newcastle upon Tyne, Newcastle upon Tyne, NE2 4HH, UK.

Introduction

Bacterial cells display a multiplicity of forms that are important for their function or survival (Young, 2006). The generation of these forms relies on the temporal and spatial regulation of cell growth and division. How this is achieved is not well understood. In bacteria, growth is typically linked to the growth of the peptidoglycan (PG) cell wall, also referred to as the sacculus (Höltje, 1998; Vollmer and Höltje, 2001; Cabeen and Jacobs-Wagner, 2005). The PG sacculus is a single, giant molecule, composed of a network of glycan strands cross-linked by peptides, which encases the cytoplasmic membrane.

Rod-shaped bacteria undergo two phases of growth, a cell elongation phase during which the cell laterally expands while maintaining its width, and a cell division phase, which leads to the formation of new cell poles. The prevailing view suggests that bacteria use different modes of PG growth for elongation and division. Cell elongation is thought to occur by dispersed or helical insertion of new PG material into the pre-existing polymer along the sidewalls, except at the poles (Burman *et al*., 1983; Mobley *et al*., 1984; Woldringh *et al*., 1987; de Pedro *et al*., 1997; Daniel and Errington, 2003); whereas cell division proceeds by localized PG synthesis at the site of division. After division, PG metabolism at the newly formed poles is believed to be shut down to restore PG growth along the entire sidewalls of the daughter cells. There are a few exceptions to this rule such as *Corynebacterium*, a rod-shaped bacterium, which primarily elongates by polar growth derived from division (Umeda and Amako, 1983; Daniel and Errington, 2003).

The bacterial cytoskeleton affects the shape and size of the cell by virtue of its apparent role in cell elongation and division. The actin homologue MreB is involved in the elongation phase by controlling cell width during lateral expansion. Impairment of MreB function causes progressive cell widening, and ultimately, spheroid morphology (Wachi *et al*., 1987; Jones *et al*., 2001; Figge *et al*., 2004; Gitai *et al*., 2004; 2005; Kruse *et al*., 2005). Consistently, spherical bacteria (cocci) lack MreB, whereas rod-shaped bacteria have at least one *mreB* gene copy (with some rare exceptions including *Corynebacterium*, which has no *mreB* and grows from the poles) (Jones *et al*., 2001; Daniel and Errington, 2003). It has been proposed that the

helical distribution of the MreB homologue Mbl may regulate the helical PG insertion in *Bacillus subtilis* (Daniel and Errington, 2003), although this view remains debated (Tiyanont *et al*., 2006). MreB has additional functions in DNA segregation and cell polarity (Kruse *et al*., 2003; Soufo and Graumann, 2003; Gitai *et al*., 2004; 2005; Shih *et al*., 2005).

While MreB is involved in cell elongation, the tubulin homologue FtsZ is thought to be specific to the division phase. It has been shown in *Escherichia coli*, *B. subtilis*, *Caulobacter crescentus* and several other bacteria that when FtsZ function is lost, division is prevented whereas cell elongation continues, leading to cell filamentation (Beall and Lutkenhaus, 1991; Dai and Lutkenhaus, 1991; Wang *et al*., 2001). FtsZ assembles into a ring-like structure at the future site of division where it recruits other cell division proteins (Bi and Lutkenhaus, 1991; Errington *et al*., 2003; Goehring and Beckwith, 2005; Shih and Rothfield, 2006). FtsZ ring constriction promotes localized, septal PG synthesis and leads to cytokinesis and pole formation.

Here we describe an additional, active role for the FtsZ ring in cell elongation and thus cell shape determination.

Results and discussion

Caulobacter crescentus *PG sacculus elongates from a central region*

The current view on cell elongation in bacteria heavily relies on PG growth studies done on very few model organisms using asynchronous cell populations. Notably, *E. coli*, which elongates by a dispersed (or patchy) mode of PG growth along the sidewalls (de Pedro *et al*., 1997), has been the reference for Gram-negative bacteria. To gain more temporal resolution on PG growth during the cell cycle, we sought to examine the growth of *C. crescentus* as synchronized cell cycle populations of this Gram-negative bacterium can be easily obtained (Evinger and Agabian, 1977). The *C. crescentus* cell cycle is also conveniently associated with morphological events that include the elongation of a new born flagellated 'swarmer cell' into a 'stalked cell'. During this transition, the polar flagellum is lost and replaced by a stalk, which is a thin extension of the cell envelope. After elongation of the stalked cell, cell division occurs asymmetrically to produce a swarmer cell and a slightly longer stalked cell. Because of this size asymmetry, the longer, stalked progeny has a shorter elongation phase as it skips the period of growth that the swarmer progeny uses to become a stalked cell (Terrana and Newton, 1975). *C. crescentus* cells have a vibrioid (curved-rod) morphology and its cell curvature requires the intermediate filament-like protein crescentin (Ausmees *et al*., 2003). Apart from these asymmetric particularities, *C. crescentus* is similar to *E. coli* and other non-spherical bacteria in the sense that it undergoes a cell elongation phase before dividing. *C. crescentus* also contains MreB and FtsZ homologues with known localizations (Kelly *et al*., 1998; Figge *et al*., 2004; Gitai *et al*., 2004; Thanbichler and Shapiro, 2006). As expected, loss of MreB and FtsZ function result in spheroid and filamentous cell phenotypes respectively.

While fluorescent antibiotic derivatives such as vancomycin can be used to stain the sites of nascent PG growth in *B. subtilis* and other Gram-positive bacteria (Daniel and Errington, 2003; Tiyanont *et al*., 2006), the outer membrane of Gram-negative bacteria typically presents a permeability barrier against these probes. Surprisingly, *C. crescentus* has been reported to be sensitive to vancomycin (Johnson and Ely, 1977). However, *C. crescentus* PG contains a high level of pentapeptides that are recognized by vancomycin (Markiewicz *et al*., 1983). The fluorescent vancomycin labelling method is thus not suitable for PG growth studies in *C. crescentus* as it would label nascent as well as old PG. Therefore, we took advantage of the D-Cysteine (D-Cys) labelling method developed in *E. coli* (de Pedro *et al*., 1997), which we modified to enhance detection (see *Experimental procedures*). This method relies on the ability of the cell to incorporate exogenous D-Cys into PG by a periplasmic exchange reaction with the terminal D-alanyl residue of PG peptide chains. Once incorporated, the sacculi are then isolated and the D-Cys residues are biotinylated and modified for detection by electron microscopy (EM) or fluorescence microscopy. After uniform D-Cys labelling of the PG, the cells are resuspended in medium lacking D-Cys. Chase analysis shows where new PG growth occurs as these areas lack D-Cys label.

We found that a concentration of 125 μg ml^{-1} of D-Cys in peptone yeast extract (PYE)-rich medium had a moderate effect on *C. crescentus* growth while resulting in significant D-Cys incorporation into the PG as judged by high-performance liquid chromatography (HPLC) analysis of PG digests (data not shown). Importantly, based on optical density (OD) measurements and visual inspection of cell morphologies, cell growth and cell cycle progression appeared fully normal after D-Cys removal (data not shown), which is when growth was examined. An asynchronous population of cells was then labelled with D-Cys for about four generations after which the cells were grown for one generation in the absence of D-Cys. Before chase ($t = 0$), isolated sacculi of all cell types were uniformly and heavily labelled with D-Cys, validating this method for use in *C. crescentus* (Fig. 1A). After chase, a large area of D-Cys-clearing was often seen around the centre of sacculi (Fig. 1A), suggesting that a significant amount of PG growth occurred near midcell. The area of clearing was consistent with localized PG synthesis

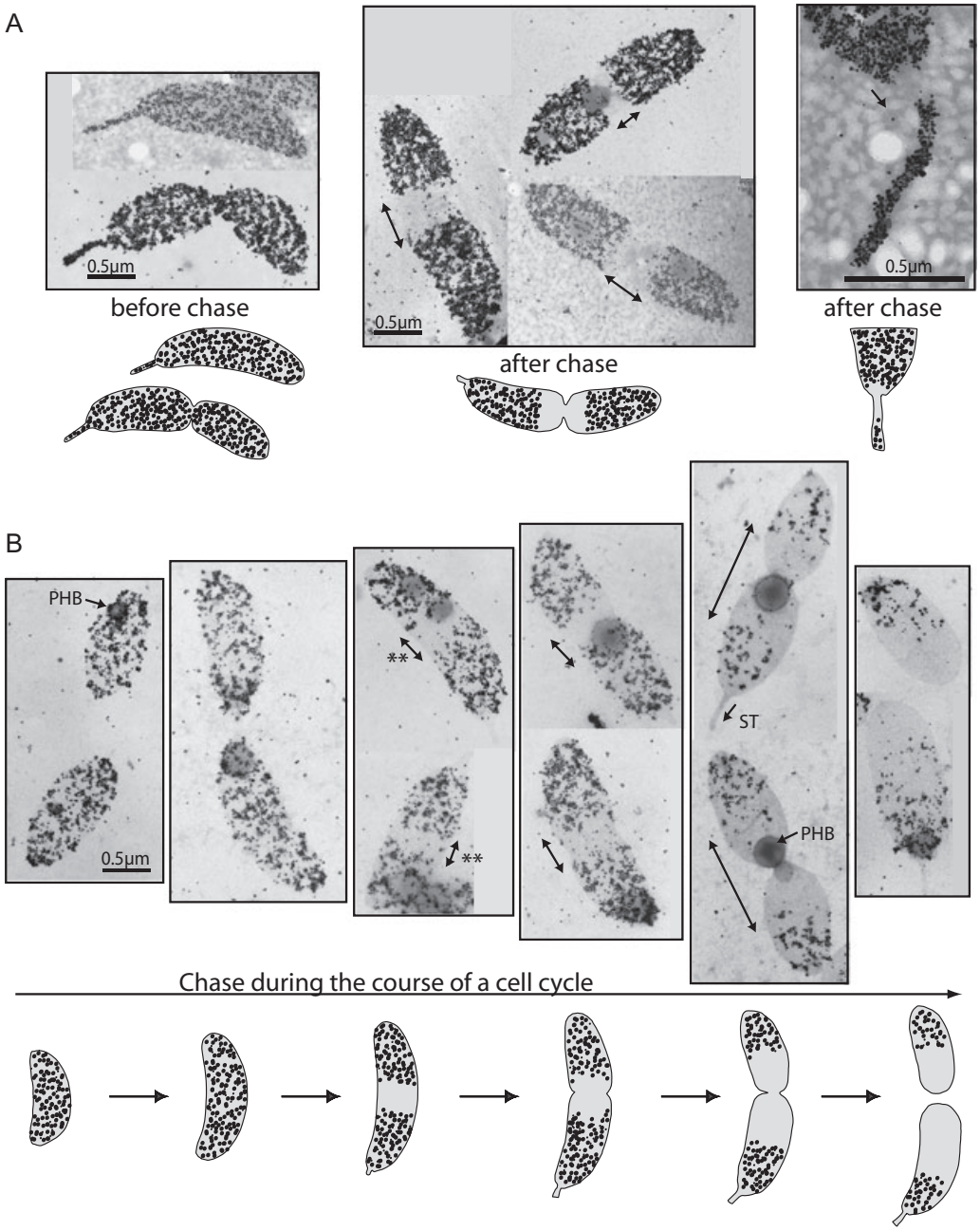

Fig. 1. *C. crescentus* elongates from the cell centre.
A. An asynchronous population of cells was labelled with D-Cys for four generations. The cells were then washed, resuspended in D-Cys-free PYE medium (to initiate the chase), and allowed to grow at 30°C for one generation. Sacculi were prepared and the D-Cys residues were labelled and visualized by EM. Areas without D-Cys (clear areas shown with arrows) represent areas of new PG growth. Schematics of D-Cys labelling are shown.
B. Cells were grown in the presence of D-Cys for four generations, and a synchronous population of swarmer cells was then isolated. These swarmer cells were allowed to progress through the cell cycle in the absence of D-Cys to examine growth during the cell cycle. Sacculi were prepared and the D-Cys residues were labelled and visualized by EM. Clearing near midcell indicates that a significant amount of growth occurs from the midcell region (double-sided arrows). Schematics of D-Cys labelling are shown. Double asterisks (**), medial clearing with no visible constriction. ST, stalk PG free of label. PHB, poly-β-hydroxybutyrate granule.

occurring during division and cell pole formation. The D-Cys clearing from the base of the stalk (Fig. 1A) confirmed that stalk formation and elongation proceeds by localized incorporation of new PG at the base of the stalk, which is consistent with tritiated glucose labelling studies (Schmidt and Stanier, 1966).

To examine in more temporal detail PG growth during cell elongation, synchronous D-Cys-labelled swarmer cell

populations were isolated and immediately chased. Sacculi were then isolated at different times during the cell cycle. Areas without D-Cys label therefore marked growth that had occurred since the beginning of the swarmer cell cycle. Sacculi from cells in early stages of the cell cycle were uniformly labelled with D-Cys [Fig. 1B; note that *C. crescentus* sacculi typically contained granules of poly-β-hydroxybutyrate, a storage polymer, which appeared as dark inclusions in EM images (Poindexter and Hagenzieker, 1982)]. During the course of the chase, a significant amount of D-Cys clearing appeared at the centre of the sacculi (Fig. 1B). Strikingly, this medial clearing was readily apparent in sacculi lacking any visible constriction (Fig. 1B, double asterisks). The wide, medial gap of D-Cys label in the non-constricting sacculi (see Fig. S1 for additional micrographs) argued against the possibility that this massive PG synthesis contributes to the formation of new poles during cell division; instead it showed that a significant amount of growth occurs from midcell in *C. crescentus*. The amount of D-Cys clearing increased in sacculi from constricting cells, consistent with localized PG growth for pole formation. Sacculi isolated from daughter cells following division lacked D-Cys label over almost half their length. The D-Cys data indicate that not only cell division, but also cell elongation derive in significant part from localized PG synthesis near midcell in *C. crescentus*.

In the absence of FtsZ, C. crescentus *elongates via PG growth along the entire sidewalls*

As a significant amount of PG growth occurs near midcell during cell elongation, we speculated that this localized growth may require the FtsZ ring, which assembles in the stalked cell stage (Kelly *et al*., 1998; Thanbichler and Shapiro, 2006). If true, another mode of growth, corresponding approximately to the swarmer-to-stalked cell transition, must account for cell elongation occurring before FtsZ ring assembly. This mode of growth would also contribute to the cell elongation that leads to cell filamentation in FtsZ-depleted cells (Wang *et al*., 2001).

The D-Cys labelling technique was not sufficiently sensitive to examine with confidence the short period of PG growth occurring before FtsZ assembly (swarmer-to-stalked cell transition phase). To expand this period of growth, we prevented FtsZ assembly by depleting the cells of FtsZ and allowed the cells to elongate into filaments for PG growth analysis. Specifically, cells expressing *ftsZ* under the xylose-inducible promoter (YB1585) were grown for approximately four generations in the presence of D-Cys. During the last hour of D-Cys labelling, FtsZ depletion was initiated by replacing xylose in the medium with glucose. At time zero (corresponding to the time of D-Cys removal) and after a 2 h chase period, sacculi were isolated and examined by fluorescence

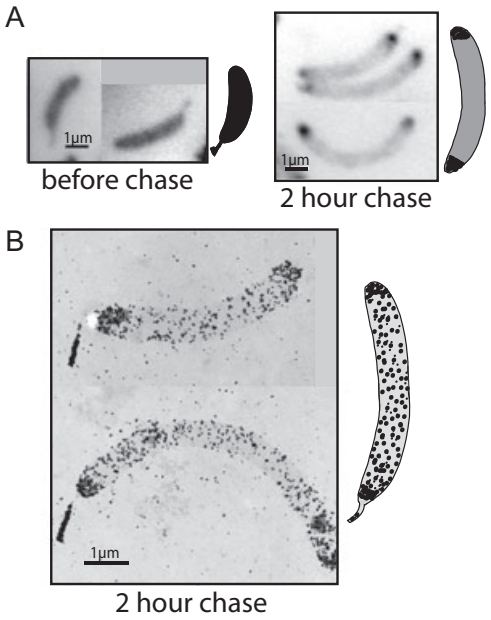

Fig. 2. Zonal PG growth during cell elongation is FtsZ-dependent. YB1585 cells were labelled with D-Cys for four generations. During the last hour of labelling, FtsZ depletion was initiated by resuspending cells in medium lacking xylose and containing glucose. After D-Cys labelling, cells were grown in the absence of D-Cys (chase) to examine the mode of PG growth under FtsZ depletion conditions. Sacculi were then prepared and the D-Cys residues were labelled.
A. Fluorescence microscopy shows that before chase, the sacculi were uniformly labelled with D-Cys. After 2 h of chase, the D-Cys label was fairly homogenously diluted along the entire cylindrical part of the sacculi while the poles remained heavily labelled.
B. Electron microscopy examination of sacculi from 2 h chased cells shows a dilution of the D-Cys label over the entire sidewalls except at the poles. The part of the stalk close to the cell body is free of label whereas the remainder of the stalk remains heavily labelled.

microscopy and EM. At time zero (before chase), the sacculi were uniformly labelled as expected (Fig. 2A). After chase, only the poles remained heavily labelled whereas the cylindrical walls showed a weak labelling (Fig. 2A and B). The absence of wide, unlabelled gaps and the fairly homogenous dilution of the label over the cylindrical walls indicate that in the absence of FtsZ, PG synthesis is dispersed over the sidewalls and is no longer localized near midcell. The heavy polar label suggests little or no PG growth at the poles of FtsZ-depleted cells, as it is observed in *E. coli ftsZ* mutants (Woldringh *et al*., 1987; de Pedro *et al*., 1997).

These findings are consistent with the idea that before FtsZ assembly near midcell (swarmer) cells grow via dispersed PG insertion over the entire sidewalls. After FtsZ assembles into a ring structure, which occurs early into the stalked cell stage (Kelly *et al*., 1998; Thanbichler and Shapiro, 2006), the cells elongate (at least in large part) by localized, FtsZ-dependent PG synthesis from the central cell region.

MurG colocalizes with the FtsZ ring during cell elongation

While a major function for FtsZ in cell wall elongation was surprising, its role in directing septal PG synthesis during cell division had been well documented (Woldringh *et al*., 1987; de Pedro *et al*., 1997; Daniel and Errington, 2003). The FtsZ ring is thought to serve as a scaffold for the recruitment of cell division proteins, including penicillin-binding proteins (PBPs) involved in the biogenesis of the PG polymer (Goehring and Beckwith, 2005; Shih and Rothfield, 2006). While most studies have focused on the localization of PBPs, we speculated that the FtsZ ring may be involved in an earlier step in PG biogenesis by affecting where synthesis of the lipid-linked disaccharide-pentapeptide PG precursor (known as lipid II) occurs. Lipid II is essential for any form of PG synthesis (used for elongation or division) and the final step in its formation is catalysed by the conserved MurG enzyme, a peripheral protein associated with the cytoplasmic face of the inner membrane (Mengin-Lecreulx *et al*., 1991).

To test our hypothesis, we examined the localization of FtsZ and MurG in synchronized cell populations using a strain (CJW1572) carrying a chromosomally encoded *ftsZ–mCherry* fusion (under the vanillate-inducible promoter) and a *murG–mgfp* fusion (under the native *murG* promoter as the only functional and chromosomal *murG* copy) (Fig. 3A). At the start of the swarmer cell cycle, FtsZ–mCherry initially formed a polar focus as previously described (Thanbichler and Shapiro, 2006). At this point, MurG–mGFP had a dispersed, although non-homogenous, distribution (see Fig. S2 for a larger image). However, shortly after FtsZ ring formation (which appeared as a band by epifluorescence microscopy), MurG–mGFP accumulated near midcell and colocalized with FtsZ–mCherry (Fig. 3A). This colocalization occurred before any visible signs of cell constrictions as judged by differential interference contrast (DIC) microscopy and EM analyses (Fig. 3A). About halfway into the cell cycle, cell constrictions started to appear. Thereafter, the MurG–mGFP and FtsZ–mCherry bands progressively and concomitantly constricted until they became foci. Before cell separation, MurG–mGFP delocalized to re-adopt a diffuse distribution in late pre-divisional cells (Fig. 3A). As *C. crescentus* divides via a constriction mechanism (Poindexter and Hagenzieker, 1981), a cell indentation is a visible sign of PG growth leading to pole formation. Thus, MurG and FtsZ colocalize near midcell well before the appearance of a cell indentation, suggesting a high synthesis and thereby availability of lipid II PG precursors at the FtsZ ring location. This is consistent with our D-Cys data showing that localized PG synthesis near midcell contributes to cell elongation soon after FtsZ ring assembly. Similarly to what has been observed for MurG in *E. coli* (Mengin-Lecreulx *et al*., 1991), biochemical fractionation (Fig. 3D) showed that our MurG–mGFP fusion was mostly membrane-associated in *C. crescentus* (which cannot be appreciably seen by epifluorescence microscopy when the cells are small and the fluorescence signals are weak).

It has been shown that the helical structure of MreB condenses into an FtsZ-dependent ring-like structure at the future site of division in *C. crescentus* (Figge *et al*., 2004; Gitai *et al*., 2004). The reason for this rearrangement has remained mysterious. Our findings suggest that this is linked to a considerable redirection of PG synthesis to the FtsZ ring location soon after FtsZ ring assembly. Using time-course microscopy, we confirmed that MreB and FtsZ colocalize near midcell soon after FtsZ assembles into a ring by imaging cells (CJW1484) that produced both GFP–MreB and FtsZ–mCherry (Fig. 3B).

Statistics on the localization of GFP–MreB and MurG–mGFP near midcell relative to that of FtsZ–mCherry and to the presence of cell indentation are also provided in graphical form (Fig. 3C). This pairwise comparison (using the formation of the FtsZ ring as a temporal and spatial reference) showed that MurG and MreB colocalize with FtsZ shortly after FtsZ assembles near the centre of the cell and well before cell constriction begins. MreB, MurG and FtsZ retain this near-medial colocalization until a late pre-divisional cell stage when first MreB and later MurG delocalize from the site of FtsZ ring constriction.

Time-lapse microscopy of CJW1572 and CJW1484 confirmed this temporal sequence (Movies S1 and S2; note that under the time-lapse growth conditions, the cell cycle is about 210 min versus 100 min for the time-course experiments shown in Fig. 3 because of differences in medium composition and growth temperature). The time-lapse Movie S1 also shows that division yields a swarmer daughter cell with polarly localized FtsZ–mCherry and dispersed MurG–mGFP, restarting the cycle. In the stalked daughter cell, however, FtsZ–mCherry localizes near midcell almost immediately after division and is shortly followed by MurG–mGFP. This suggests that the stalked daughter cell primarily elongates by zonal, FtsZ-dependent growth.

MurG localization near midcell requires the FtsZ ring but not the MreB ring

As colocalization of MurG, MreB and FtsZ near midcell suggested an intimate association between these proteins, we next tested whether the localization of MurG–mGFP near midcell requires FtsZ and/or MreB. A strain (CJW1607) carrying *ftsZ* under xylose-inducible expression and *murG–mgfp* under endogenous expression was grown in the presence of xylose. Swarmer cells were then isolated and resuspended in medium with glucose (and no xylose), causing FtsZ depletion. Under these conditions,

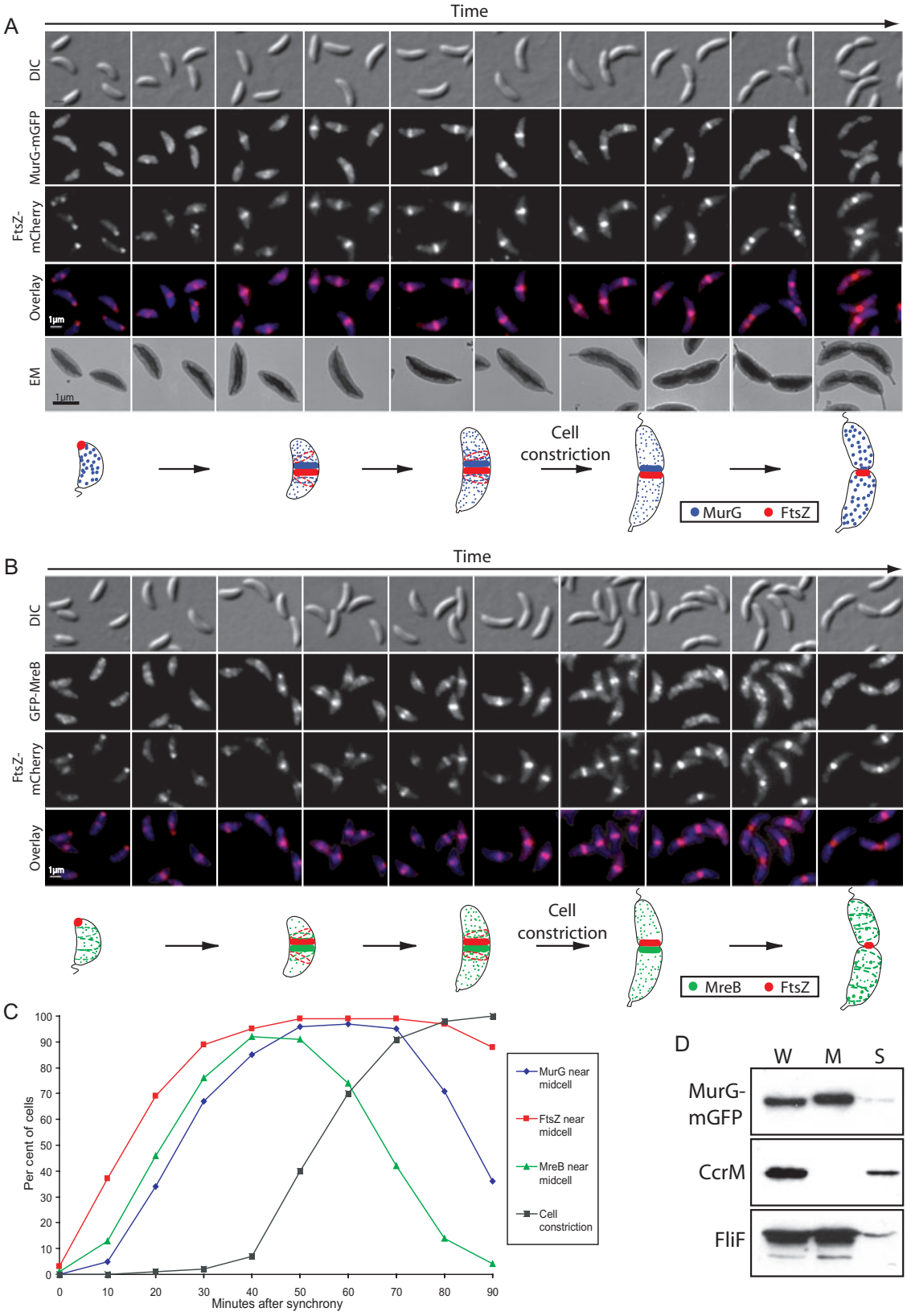

Fig. 3. Relative localization of fluorescently labelled MurG, MreB and FtsZ during the cell cycle.
A. Synchronized CJW1572 swarmer cell populations producing MurG–mGFP and FtsZ–mCherry were resuspended in PYE liquid medium to resume growth at 30°C. After resuspension and every 10 min after, a sample was examined by DIC and fluorescence microscopy. In parallel, a sample was prepared for EM analysis. Under these time-course conditions, the cell cycle takes about 100 min. Schematics showing the temporal sequence of protein localization and cell constriction are given.
B. Synchronized CJW1484 swarmer cell populations producing GFP–MreB and FtsZ–mCherry were treated as in (A).
C. Per cent of cells with visible constrictions and with MurG–mGFP, GFP–MreB and FtsZ–mCherry localizations near midcell were plotted as a function of time during a cell cycle of about 100 min. Protein localization and constriction patterns were examined using synchronized population of strains CJW1484 and CJW1572. At least three independent time-course experiments were performed for each strain and over 150 cells were considered for each time point. In the case of FtsZ–mCherry localization and constrictions, values for strains CJW1572 and CJW1484 were averaged.
D. Subcellular localization of MurG–mGFP. A whole cell lysate (W), soluble fraction (S) and membrane fraction (M) were isolated and analysed as described in *Experimental procedures*. CcrM, a cytoplasmic protein (Stephens *et al*., 1997), and FliF, a membrane-bound protein (Jenal and Shapiro, 1996), serve as quality controls for the soluble and membrane fractions respectively.

MurG–mGFP failed to accumulate as a distinguishable band, but instead remained diffusely distributed throughout the entire length of FtsZ-depleted cells (Fig. 4A and Movie S3).

To test whether the fairly dispersed pattern of MurG–mGFP was due to the loss of the FtsZ ring and not cell filamentation, we treated CJW1576 swarmer cells with cephalexin (2.5 μg ml^{-1}) which affects a later cell division step. After 3 h of cephalexin treatment, FtsZ–mCherry often localized off-centred at alternative sites such as quarter positions within the elongated cells; MurG–GFP was found to colocalize with FtsZ at these positions as well (Fig. 4B). This lends further support to the idea that MurG localization is linked to and dependent on the FtsZ ring localization. All together, our data suggest that formation of the FtsZ ring mediates the accumulation of MurG near midcell.

Formation of the MreB ring near midcell is also abolished in FtsZ-depleted cells (Figge *et al*., 2004), suggesting the possibility that MurG is recruited to the FtsZ structure via MreB. However, MurG–mGFP mostly retained its ability to colocalize with the FtsZ structure after treatment with A22, a drug known to disrupt the MreB cytoskeleton within minutes of treatment (Gitai *et al*., 2005). The A22 treatment was initiated in swarmer cells when MurG–mGFP had a dispersed localization and FtsZ–mCherry was mostly polar (Fig. 4C). A22 slowed cell growth, causing FtsZ assembly near midcell to occur at a later time point after synchronization. Importantly, with or without A22, MurG–mGFP colocalized with the FtsZ–mCherry ring soon after its formation and well before cell constriction initiation (Fig. 4C). One concern, however, was that even with a concentration of 10 μg ml^{-1} of A22, we could still distinguish a faint GFP–MreB accumulation near midcell in some cells (Fig. S3). Higher concentrations of A22 failed to resolve this problem while further retarding cell growth (data not shown). As the A22 drug experiments were not entirely conclusive, we sought to generate a MreB mutant that fails to localize near midcell and to test whether MurG can still colocalize with the FtsZ ring under this condition. To obtain this MreB mutant, we were tipped off by a recent study describing the isolation of *mreB* mutations that confer resistance to A22 (10 μg ml^{-1}) (Gitai *et al*., 2005). Interestingly, one of these mutations was shown to produce a MreB protein ($MreB_{T167A}$), at least in part, defective in localizing into a medial band; this *mreB* mutation, however, also gave rise to a minor filamentation phenotype (Gitai *et al*., 2005). As it was unclear whether the cell division defect and the localization deficiency of $MreB_{T167A}$ had a causal relationship, we isolated *mreB* mutants that grew on plates in the presence of a lower concentration of A22 (5 μg ml^{-1}) and visually screened for mutants with fairly normal cell size and shape. One of them (CJW1715; see Fig. S4 for a DIC image) had a mutation in *mreB* causing a Gln to Pro substitution at position 26 in MreB. Fluorescence microscopy revealed that $MreB_{Q26P}$ failed to accumulate as a band (ring) near midcell at any time during the cell cycle; instead the mutant protein formed distinct patches whose subcellular distribution changed rapidly over time (Fig. 4D; Movie S4). Despite the inability of $MreB_{Q26P}$ to form a ring, MurG–GFP colocalized with the FtsZ ring at or soon after its assembly in the $mreB_{Q26P}$ mutant, strongly arguing that MurG is not recruited to the FtsZ ring via MreB (Fig. 4E; Movie S5).

MurG can still colocalize with the FtsZ ring after treatment with fosfomycin

Similarly to A22, fosfomycin treatment did not appear to significantly affect the recruitment of MurG–mGFP to the FtsZ–mCherry ring. Fosfomycin specifically inhibits MurA, a cytoplasmic enzyme upstream of MurG in the PG biosynthesis pathway (Kahan *et al*., 1974). Without MurA activity, MurG′ substrate is no longer formed. Addition of 20 μg ml^{-1} of fosfomycin to CJW1572 was sufficient to completely arrest growth after 2 h of exposure (Fig. S5), suggesting that within that time, the pool of PG precursors was entirely depleted, depriving MurG of its substrate. We observed 77% of total cells ($n = 62$) showing colocalization between MurG–mGFP and FtsZ–mCherry after 2 h of fosfomycin treatment (Fig. 4F), relative to 86% in the

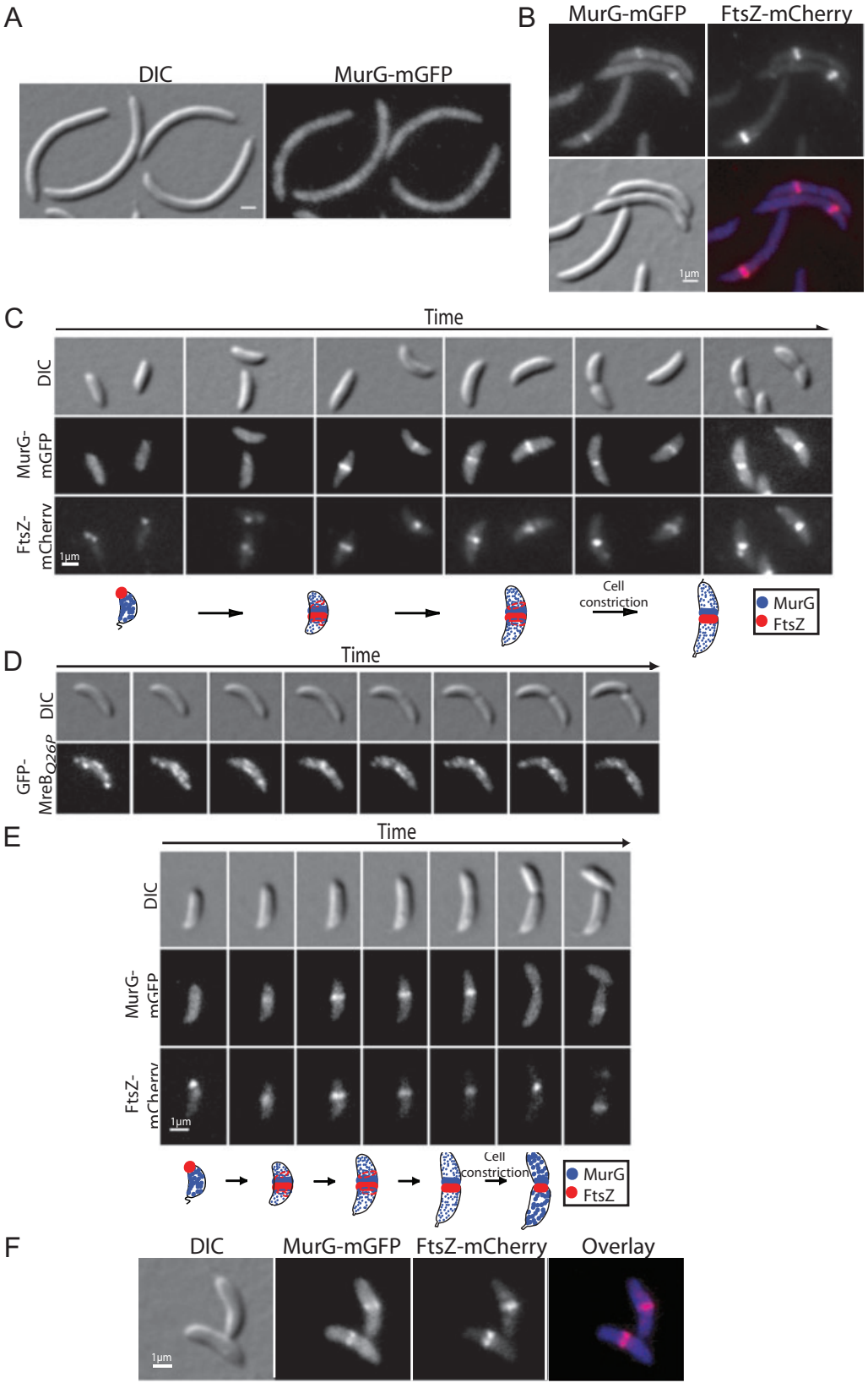

Fig. 4. MurG localization near midcell is dependent on FtsZ and independent of MreB.
A. Swarmer cells of CJW1607 were grown in the absence of xylose and presence of glucose to shut-off *ftsZ* expression and block cell division. Under these conditions, MurG–mGFP failed to accumulate as a distinguishable band as examined by fluorescence microscopy. The dispersed localization of MurG–mGFP is shown after 3 h of FtsZ depletion.
B. Strain CJW1576 was grown for 2 h in the presence of 0.5 mM vanillic acid to induce *ftsZ–mCherry* expression. Swarmer cells were then isolated and resuspended in PYE medium containing cephalexin (2.5 μg ml^{-1}) and vanillic acid. After 3 h of cephalexin treatment, the cells were elongated and fluorescence microscopy showed that FtsZ–mCherry often localized off-centred and MurG–GFP colocalized with FtsZ at these positions.
C. A CJW1572 cell culture was treated with 0.5 mM vanillic acid to induce *ftsZ–mCherry* expression 2 h before synchronization. Swarmer cells were then isolated and resuspended in PYE medium containing A22 (10 μg ml^{-1}) and vanillic acid. A sample was examined by fluorescence microscopy every 15 min to examine the localization of MurG–mGFP and FtsZ–mCherry during growth.
D. CJW1682 cells were treated with 0.3% xylose for 3 h. A sample was placed on an agarose-padded slide containing M2^{+} and 0.3% xylose and cells were examined by fluorescence microscopy every 5 min to examine the localization of GFP–MreB$_{Q26P}$ during growth. Selected images are shown; for the full time-lapse sequence, see Movie S4.
E. CJW1998 cells carrying the *mreB$_{Q26P}$* mutation were grown in M2G^{+} and treated for 3 h with 0.5 mM vanillic acid to induce *ftsZ–mCherry* expression. A sample was placed on an agarose-padded slide containing M2G^{+} and 0.5 mM vanillic acid, and the localization of MurG–mGFP and FtsZ–mCherry was examined by fluorescence microscopy every 10 min. Selected images are shown; for the full time-lapse sequence, see Movie S5.
F. Microscopy of CJW1572 cells treated with fosfomycin (20 μg ml^{-1}) for 2 h.

absence of the antibiotic ($n = 70$). This suggests that the activity of MurG or the localization of its substrate does not determine the location of MurG. Instead, it is the FtsZ ring-like structure that soon after its formation appears to (directly or indirectly) recruit the MurG protein, thereby redirecting the synthesis of lipid II to the midcell region.

Cell poles change shape after division

Initially, we assumed that the slow constriction of the *C. crescentus* FtsZ ring, by promoting the addition of PG rings of progressively decreasing diameter, was responsible for the generation of tapered poles in this organism. By contrast, *E. coli*, which also divides by constriction (Steed and Murray, 1966; Burdett and Murray, 1974), has oblate cell poles. However, close examination of sacculi from *C. crescentus* late pre-divisional cells and newborn daughter cells (obtained from a late time point after synchrony) showed that the tapered shape of the cell pole is generated after division. In sacculi from late pre-divisional cells (97%, $n = 29$), the nascent poles (generated by ongoing cell division) had a different, less pointed (more oblate) shape relative to the existing poles (Fig. 5A). Consequently, sacculi from young daughter cells (66%, $n = 101$) had an egg shape with the new pole displaying a lower degree of curvature than the old pole (Fig. 5A). The identity of the poles (new versus old) was verified by the distribution of the D-Cys label in sacculi isolated after D-Cys labelling and chase (Fig. 5B). These observations indicate that cell division generates fairly oblate new cell poles, which become more pointed in the next cell cycle. The change in cell pole curvature did not seem to abruptly take place at a specific time following cell division; instead it appeared to occur very gradually during the course of the cell cycle of the daughter cells (data not shown). This morphologically apparent pole maturation suggests that the polar cell wall undergoes remodelling and remains metabolically active for a certain time after cell division.

Growth model during the C. crescentus *cell cycle*

Our data suggest a model in which *C. crescentus* relies on several temporally and spatially regulated modes of PG growth to define its size and shape (Fig. 6A). Cell elongation occurs via two modes of PG synthesis: dispersed PG insertion along the sidewalls and zonal PG deposition near midcell. The swarmer progeny uses the dispersed mode until halfway into the elongation phase (approximately when the cell reaches the size of the stalked progeny) when a large amount of PG synthesis is redirected to a central region of the cell. In our model, FtsZ assembly into a ring-like structure mediates this medial PG synthesis by recruiting (directly or indirectly) MurG and thereby redirecting the location of PG precursor synthesis near midcell (Fig. 6B). Some cell elongation may still occur from PG insertion along the sidewalls because some MurG signal remains dispersed even when MurG is mostly localized near midcell (Fig. 3A). Interestingly, during the elongation phase, the FtsZ ring and associated MurG are mobile (Movie S1), suggesting that lipid II may be deposited within a more or less broad central zone dictated by the FtsZ movement. Approximately halfway into the swarmer cell cycle (which corresponds to the end of the cell elongation phase), the FtsZ ring stabilizes at one position and constriction is initiated. Association of MurG with the constricting FtsZ ring results in accumulation of lipid II PG precursors at the leading edge of the invaginating cell envelope, causing the addition of PG rings of progressively decreasing diameter for the generation of new cell poles (Fig. 6A and B). At the end of the cell cycle, MurG delocalizes from the site of FtsZ constriction to reset a lateral mode of dispersed PG synthesis over the sidewalls of the future daughter cells (Fig. 6B). The smaller, swarmer daughter cell restarts the cycle described above whereas the stalked progeny quickly reforms the FtsZ ring after cell separation and uses FtsZ-directed growth as a major mode of cell wall elongation.

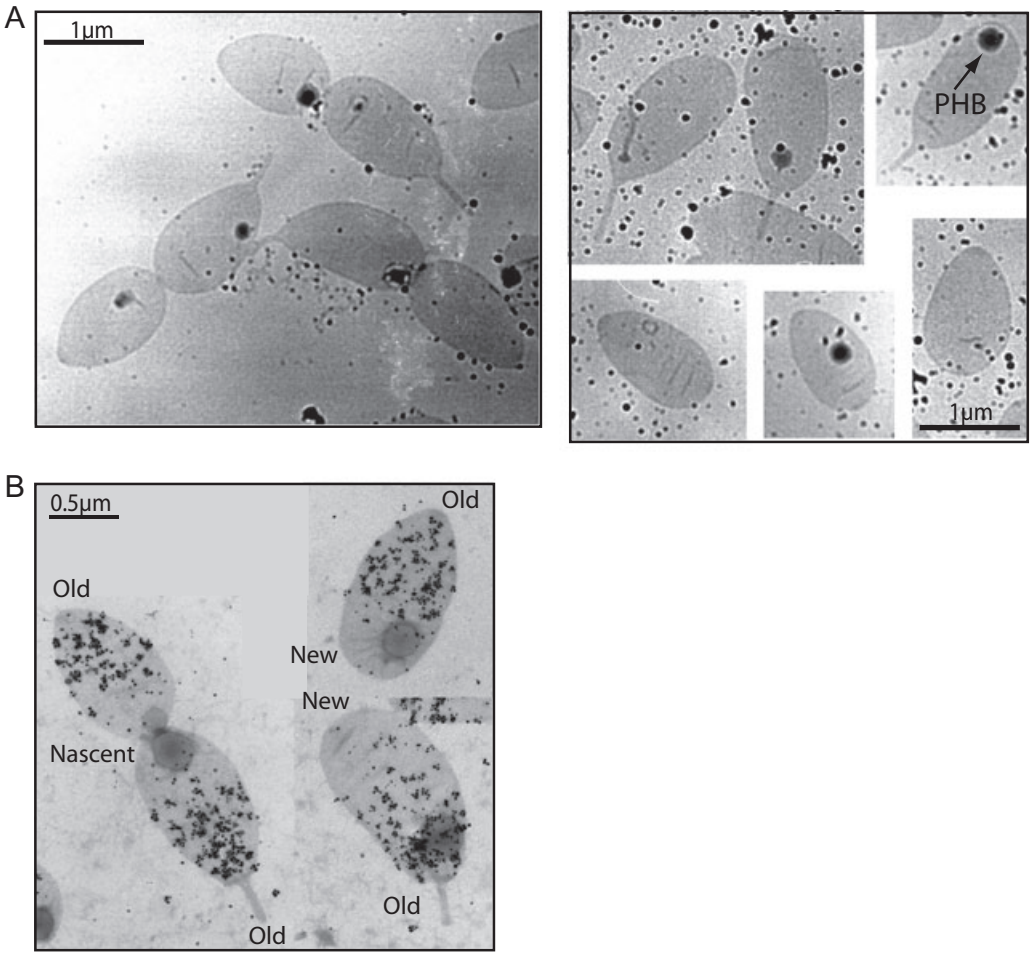

Fig. 5. Cell pole shape changes following division.
A. After synchronization, wild-type CB15N cells were resuspended in fresh liquid PYE medium and allowed to resume growth at 30°C. Sacculi were isolated from cells from a late time point that included late pre-divisional cells (left panel) and young daughter cells that had recently divided (right panel). These sacculi were stained with 1% uranyl-acetate and examined by EM. PHB, poly-β-hydroxybutyrate granule.
B. After approximately four generations of growth in PYE medium containing 125 μg ml^{-1} D-Cys, wild-type (CB15N) swarmer cells were isolated and resuspended in PYE medium free of D-Cys to initiate the chase. After approximately one generation time, sacculi were isolated and the D-Cys residues were biotinylated and modified for detection by EM. In sacculi from daughter cells, the new pole formed by the recent division was easily recognized from the old pole by the distribution of the D-Cys label.

In *B. subtilis*, PG insertion along the sidewalls has been shown to be helical (Daniel and Errington, 2003; Tiyanont *et al.*, 2006). We did not observe any evidence of helical PG insertion in *C. crescentus.* However, the limited resolution of the D-Cys method may prevent us from seeing it in the swarmer cell stage or in FtsZ-depleted cells where growth appears dispersed. Similarly, we cannot rule out the possibility that MurG has a helical, rather than dispersed, distribution in the swarmer cell stage or in FtsZ-depleted cells, as the low intensity of the MurG–mGFP fluorescent signal made three-dimensional deconvolution microscopy impractical. The observation that the MurG signal is somewhat patchy and unevenly distributed within swarmer cells (Fig. S2) may reflect some higher organization.

The synchronized mobility between MurG and the FtsZ ring in the elongation phase (Movie S1) is consistent with a close association between the two proteins. The fact that MurG does not show any strong evidence of polar localization in the swarmer cell stage [except for a polar localization in about 1–4% of cells ($n = 251$); data not shown] may indicate that MurG has a preference for the polymeric nature of the FtsZ ring or that MurG has an affinity for a protein that is specifically associated with the FtsZ ring.

Finally, we also show that the formation and the elongation of the stalk proceed by localized PG synthesis from the old pole (Fig. 6A), as previously suggested (Schmidt and Stanier, 1966). We did not observe any obvious accumulation of MurG–mGFP signal at the stalked pole, most likely because the PG synthesis involved in stalk elongation is minimal compared with the synthesis required for cell growth and pole formation.

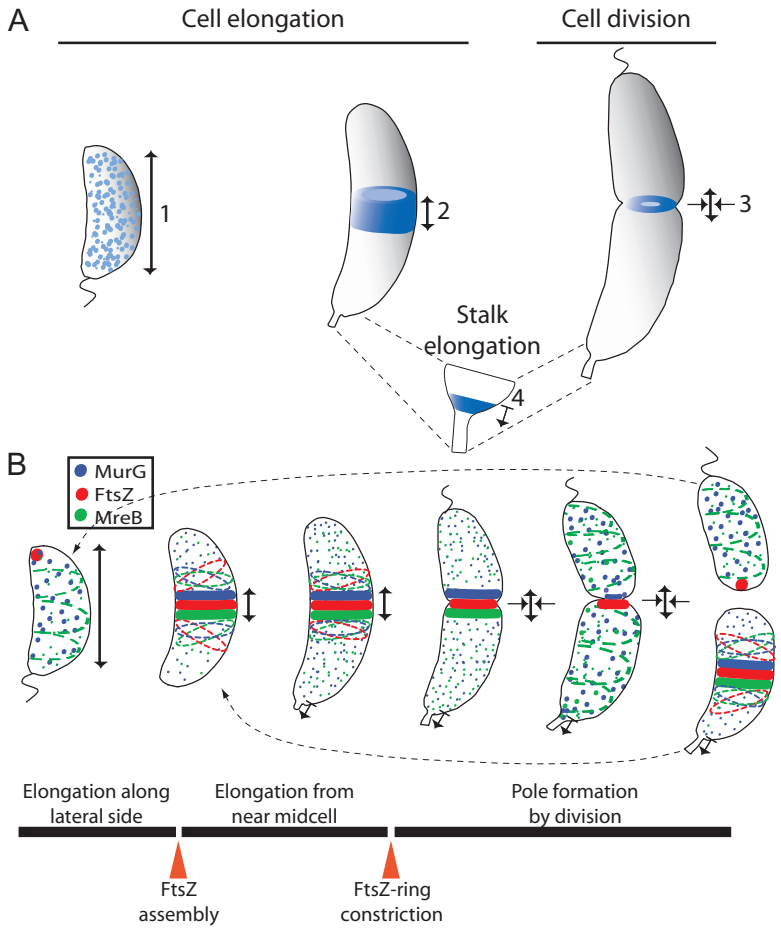

Fig. 6. Growth model during the *C. crescentus* cell cycle.
A. Several modes of PG growth occur in *C. crescentus*. The addition of new PG material and the direction of growth are depicted by blue shading and arrows respectively. (1) Dispersed insertion of new PG material into the pre-existing network along the sidewalls leads to cell elongation. (2) Zonal insertion of new PG within a constrained central region also results in lateral cell elongation. (3) Insertion of new PG at the leading edge of the invaginating cell envelope leads to pole formation. (4) Localized PG synthesis from the tip of the old pole causes outward growth and stalk elongation.
B. FtsZ-independent and FtsZ-dependent modes of growth during the cell cycle. The most prominent mode of new PG growth at each cell stage for the swarmer cell cycle is depicted with arrows. In the swarmer cell stage, FtsZ (red) has not yet assembled into a ring structure near midcell. As a result, membrane-associated MurG (blue) and MreB (green) exhibit a dispersed or helical-like distribution, resulting in cell elongation by dispersed insertion of PG precursors into the PG network along the sidewalls. The assembly of FtsZ into a ring-like structure at the stalked cell stage results in a zonal mode of PG insertion near midcell. This occurs through the recruitment of MurG to the FtsZ structure. The dispersed mode of PG growth may still occur concomitantly. The FtsZ ring-like structure and associated MurG and MreB remain in a non-constricting mode while exhibiting mobility, changing positions around midcell. Accumulation of MurG at the FtsZ ring leads to a massive accumulation and incorporation of lipid II PG precursors near midcell, which in turn results in cell elongation. About 50% into the cell cycle, the FtsZ ring and associated MurG and MreB stop moving and start constricting. Association of MurG with the FtsZ ring during constriction provides PG precursors at the leading edge of the invaginating cell envelope. Delocalization of MurG and MreB restores dispersed PG insertion in the future daughter cells. However, in the stalked progeny, elongation through zonal PG growth is quickly restored by the reassembly of the FtsZ structure and its reassociation with MurG and MreB near midcell soon after division.

A general role for FtsZ in cell elongation and cell shape determination

The cytoskeletal protein FtsZ has been thought to be dedicated to cell division and related processes. Cocci, which only grow by division, use the constricting FtsZ ring to redirect PG synthesis for the generation of a new cell hemisphere for each daughter cell (Pinho and Errington, 2003). In *Corynebacterium*, one of the few rod-shaped bacteria devoid of MreB, cell elongation occurs by polar growth derived from division (Umeda and Amako, 1983; Daniel and Errington, 2003). The role of FtsZ in this mode of growth is directly linked to its function in cell division and pole formation (Daniel and Errington, 2003). *E. coli*, *B. subtilis* and by inference other MreB-producing bacteria which constitutes the large majority of non-spherical bacteria are widely believed to elongate by a dispersed (patchy) or helical mode of PG growth along the sidewalls.

In these bacteria as in *C. crescentus*, disruption of FtsZ function blocks cell division while cell elongation and rod-shaped maintenance proceed unperturbed in appearance, leading to cell filamentation. This phenotype has led to the general belief that FtsZ does not play any active role in cell elongation. However, as we show here, the FtsZ ring directs a considerable part of cell wall elongation in *C. crescentus*, adding a new function for the FtsZ ring, one that is not connected to cell division. When FtsZ is depleted, cell elongation continues because the dispersed mode of growth takes over, hence masking the contribution of FtsZ to cell elongation. Thus, a cell filamentation phenotype associated with a loss of FtsZ function can be misleading, raising the possibility that a role for FtsZ in cell elongation may be common among bacteria.

Several lines of evidence support the idea that the FtsZ ring directs cell elongation in other bacteria. The FtsZ ring typically assembles in elongating cells before cell constriction is initiated, although the timing of this assembly varies among bacteria. In *C. crescentus*, FtsZ ring formation is triggered by the segregation of the replicated chromosomal origins, which immediately follows the initiation of DNA replication (Thanbichler and Shapiro, 2006). In *E. coli*, FtsZ ring formation coincides with the completion of DNA replication and thus occurs later during cell elongation (Den Blaauwen *et al*., 1999). Nonetheless, there is still a significant delay between the appearance of the *E. coli* FtsZ ring and the midcell localization of cell division proteins involved in septum synthesis (Aarsman *et al*., 2005). During this time interval, FtsZ could direct midcell PG elongation. Supporting this idea, old autoradiographic studies in *E. coli* showed that, while starting with a diffuse pattern, incorporation of radiolabelled PG precursors increased at midcell about 2/3 into the cell elongation phase (Taschner *et al*., 1988) at a time consistent with the time of FtsZ ring formation (Den Blaauwen *et al*., 1999). Furthermore, D-Cys pulse-chase experiments in which cell division was inhibited without affecting FtsZ ring assembly (e.g. by addition of the cell division-specific PBP3 inhibitor, aztreonam) revealed the presence of ~0.5 μm wide zones of PG synthesis at regular intervals along the filamentous cells (de Pedro *et al*., 1997). The formation of these zones required FtsZ ring function as they were absent under conditions that prevent FtsZ polymerization. As the formation of the FtsZ ring was assumed to define an early stage of cell division, it was proposed that these zones of FtsZ-dependent PG growth, then referred to as pre-septal PG, may be involved in the formation of the poles or in the differentiation of the division site in preparation for septal growth (de Pedro *et al*., 1997; Rothfield, 2003; Aarsman *et al*., 2005). In light of our findings, another possible interpretation is that, similarly to what happens in *C. crescentus* (but to a lesser extent because of the later FtsZ ring assembly in *E. coli*), the FtsZ ring contributes to lateral wall elongation in *E. coli* before division is initiated. A function for the FtsZ ring in *E. coli* cell elongation would imply a role in rod shape determination, which may become apparent only under special conditions because of the existence of the compensatory dispersed mode of PG growth. Consistent with this idea, inhibition of FtsZ function in *E. coli* causes severe cell shape abnormalities when specific PG remodelling enzymes are missing (Varma and Young, 2004).

In *Rhodobacter sphaeroides*, homologues of MreB, PBP2 and MreC, all proteins thought to affect PG metabolism, localize into a band at midcell very early during elongation, suggesting the possibility that *R. sphaeroides* primarily grows via zonal PG synthesis from midcell (Slovak *et al*., 2005; 2006). Though not verified, it is highly likely that the midcell localization of the *R. sphaeroides* proteins is dependent on FtsZ whose polymerization at midcell would presumably occur early during the *R. sphaeroides* cell cycle.

Altogether, this evidence points towards a possible widespread function for FtsZ in bacterial cell elongation. On this basis, we propose that bacteria can elongate by (dispersed or helical) PG insertion along the sidewalls and by FtsZ ring-dependent PG synthesis. The relative importance of these two modes of growth relies on the timing of FtsZ ring formation. Accordingly, the FtsZ-dependent mode of growth would be more predominant in bacteria exhibiting an early assembly of the FtsZ ring during cell elongation (e.g. *C. crescentus* and presumably *R. sphaeroides*) and less predominant when there is a late FtsZ ring assembly (e.g. *E. coli*). Thus, the mode of growth would be ultimately controlled by the specific cell cycle mechanism that regulates FtsZ assembly.

Experimental procedures

Strains, plasmids, media and growth conditions

Strains and plasmids are listed in Table S1 and the construction methods are provided in the *Supplementary material*. *C. crescentus* strains were grown at 30°C in PYE (Ely, 1991). Transformations, conjugations and transductions were used to create strains (Ely, 1991). Synchronous cell populations were obtained as previously described (Evinger and Agabian, 1977). To observe the localization of FtsZ–mCherry and GFP–MreB during the cell cycle, cultures were grown in the presence of 0.5 mM vanillic acid and 0.3% xylose for 2 h respectively, unless otherwise noted. Induction and repression of *ftsZ* was achieved by growth in the presence of 0.3% xylose and 0.2% glucose respectively.

Labelling, preparation, visualization and analysis of PG sacculi

Log phase cultures of CB15N were diluted to an OD of about 0.03 at 660 nm in PYE containing 125 μg ml^{-1} D-Cys and were

allowed to double four times. Then samples were harvested immediately, chased for one generation in the absence of D-Cys before harvesting, or synchronized and then harvested at time points throughout the cell cycle. After growth in the presence of 100 μg ml^{-1} or 125 μg ml^{-1} D-Cys, samples from the FtsZ depletion strain (YB1585) were harvested immediately or chased for two generations in the absence of D-Cys. All samples were harvested by centrifugation at 4°C and sacculi were purified and reduced as previously described (de Pedro *et al*., 1997) with minor modifications. For EM observations, samples were immobilized on nickel grids (400 mesh) and incubated with rabbit anti-biotin antiserum (kindly provided by M.A. de Pedro) as described (de Pedro *et al*., 1997; 2003). After four washes with PBG [(0.5% bovine serum albumin, 0.2% gelatine in phosphate-buffered saline (PBS)], the grids were incubated for 1 h with a 1:100 dilution of a goat Fab-anti-rabbit IgG coupled to 1.4 nm gold particles (Nanogold #2004, Nanoprobes, Yaphank, NY, USA). The grids were then washed with PBG (twice), PBS (twice) and water (thrice), and were fixed with 0.5% gluteraldehyde for 10 min, followed by another three washes with water. Silver enhancement was performed as described (Danscher, 1981). Uranyl acetate staining and EM visualization were performed as described (de Pedro *et al*., 1997). For immunofluorescence observations, samples were labelled with AMCA (7-amino-4-methylcoumarin-3-acetic acid) and observed with a UV filter. For analysis of PG digests (muropeptides), sacculi preparation, digestion with cellosyl, reduction of the muropeptides with sodium borohydride, and HPLC analysis were performed as described (Glauner, 1988; Glauner *et al*., 1988).

Microscopy

For time-course experiments, cell populations were grown in liquid cultures in rich PYE medium, synchronized when appropriate, resuspended in PYE medium containing vanillic acid and xylose as appropriate, incubated at 30°C, and viewed on M2G-agarose-padded slides. For time-lapse experiments, cells were grown in minimal M2G^{+} medium instead of PYE, synchronized when appropriate, spotted on 1% agarose-padded slides containing M2G^{+} and appropriate inductants, and viewed at room temperature (~22°C) (Lam *et al*., 2006). Auto-focusing on the DIC image was performed before image acquisition. Samples were observed using a Nikon E1000 microscope through a DIC 100× objective with a Hamamatsu Orca-ER LCD camera. Images were taken and processed with Metamorph software (Universal Imaging, PA). For EM imaging, cells (fixed with 2.5% formaldehyde) or sacculi were spotted on glow-discharged carbon-coated grids, stained with 1% uranyl acetate, and imaged on a Zeiss EM10C transmission EM (80 or 50 kV respectively).

Biochemical fractionation

Biochemical fractionation was performed as described (Figge *et al*., 2004), with the following modifications. Membranes were isolated from a log-phase culture of CJW1561 by centrifugation at 150 000 *g* for 2 h, and the final pellet was resuspended in buffer containing 1% SDS. Proteins from equal portions of whole cell lysate, membrane fraction, and soluble fraction were separated by SDS–PAGE. Immunoblot analysis was performed using α-GFP JL-8 (Clontech, CA; 1/1000), α-CcrM (1/2000) and α-FliF (1/5000).

Acknowledgements

We are grateful to Martin Thanbichler, Nathan Hillson, Lucy Shapiro and Yves Brun for strains, Barry Piekos for assistance with the EM, Mathieu Pucheault and Craig Crews for synthesis of A22, the members of the Jacobs-Wagner laboratory for critical reading of this manuscript, and Miguel A. de Pedro for the anti-biotin antibody, helpful discussion, and technical advice on the D-Cys detection technique. This work was supported by a Howard Hughes Medical Institute Predoctoral Fellowship (to M.A.), a Belgian American Educational Foundation and D. Collen Research Foundation vzw Fellowship (to G.C.), the 'Deutsche Forschungsgemeinschaft (DFG)' within the 'Forschergruppe Bakterielle Zellhülle (FOR 449)' (to W.V.), the European Commission EUR-INTAFAR (LSHM-CT-2004-512138) network (to W.V.), National Institutes of Health Grants GM065835 and GM076698 (to C.J.-W.), and the Pew Scholars Program in the Biological Sciences sponsored by the Pew Charitable Trust (to C.J.-W.).

References

Aarsman, M.E., Piette, A., Fraipont, C., Vinkenvleugel, T.M., Nguyen-Disteche, M., and den Blaauwen, T. (2005) Maturation of the *Escherichia coli* divisome occurs in two steps. *Mol Microbiol* **55:** 1631–1645.

Ausmees, N., Kuhn, J.R., and Jacobs-Wagner, C. (2003) The bacterial cytoskeleton: an intermediate filament-like function in cell shape. *Cell* **115:** 705–713.

Beall, B., and Lutkenhaus, J. (1991) FtsZ in *Bacillus subtilis* is required for vegetative septation and for asymmetric septation during sporulation. *Genes Dev* **5:** 447–455.

Bi, E.F., and Lutkenhaus, J. (1991) FtsZ ring structure associated with division in *Escherichia coli*. *Nature* **354:** 161–164.

Burdett, I.D., and Murray, R.G. (1974) Septum formation in *Escherichia coli*: characterization of septal structure and the effects of antibiotics on cell division. *J Bacteriol* **119:** 303–324.

Burman, L.G., Raichler, J., and Park, J.T. (1983) Evidence for diffuse growth of the cylindrical portion of the *Escherichia coli* murein sacculus. *J Bacteriol* **155:** 983–988.

Cabeen, M.T., and Jacobs-Wagner, C. (2005) Bacterial cell shape. *Nat Rev Microbiol* **3:** 601–610.

Dai, K., and Lutkenhaus, J. (1991) ftsZ is an essential cell division gene in *Escherichia coli*. *J Bacteriol* **173:** 3500–3506.

Daniel, R.A., and Errington, J. (2003) Control of cell morphogenesis in bacteria: two distinct ways to make a rod-shaped cell. *Cell* **113:** 767–776.

Danscher, G. (1981) Histochemical demonstration of heavy metals. A revised version of the sulphide silver method suitable for both light and electronmicroscopy. *Histochemistry* **71:** 1–16.

Den Blaauwen, T., Buddelmeijer, N., Aarsman, M.E., Hameete, C.M., and Nanninga, N. (1999) Timing of FtsZ assembly in *Escherichia coli*. *J Bacteriol* **181:** 5167–5175.

Ely, B. (1991) Genetics of *Caulobacter crescentus*. *Methods Enzymol* **204:** 372–384.

Errington, J., Daniel, R.A., and Scheffers, D.J. (2003) Cytokinesis in bacteria. *Microbiol Mol Biol Rev* **67:** 52–65.

Evinger, M., and Agabian, N. (1977) Envelope-associated nucleoid from *Caulobacter crescentus* stalked and swarmer cells. *J Bacteriol* **132:** 294–301.

Figge, R.M., Divakaruni, A.V., and Gober, J.W. (2004) MreB, the cell shape-determining bacterial actin homologue, co-ordinates cell wall morphogenesis in *Caulobacter crescentus*. *Mol Microbiol* **51:** 1321–1332.

Gitai, Z., Dye, N., and Shapiro, L. (2004) An actin-like gene can determine cell polarity in bacteria. *Proc Natl Acad Sci USA* **101:** 8643–8648.

Gitai, Z., Dye, N.A., Reisenauer, A., Wachi, M., and Shapiro, L. (2005) MreB actin-mediated segregation of a specific region of a bacterial chromosome. *Cell* **120:** 329–341.

Glauner, B. (1988) Separation and quantification of muropeptides with high-performance liquid chromatography. *Anal Biochem* **172:** 451–464.

Glauner, B., Höltje, J.V., and Schwarz, U. (1988) The composition of the murein of *Escherichia coli*. *J Biol Chem* **263:** 10088–10095.

Goehring, N.W., and Beckwith, J. (2005) Diverse paths to midcell: assembly of the bacterial cell division machinery. *Curr Biol* **15:** R514–R526.

Höltje, J.V. (1998) Growth of the stress-bearing and shape-maintaining murein sacculus of *Escherichia coli*. *Microbiol Mol Biol Rev* **62:** 181–203.

Jenal, U., and Shapiro, L. (1996) Cell cycle-controlled proteolysis of a flagellar motor protein that is asymmetrically distributed in the *Caulobacter* predivisional cell. *EMBO J* **15:** 2393–2406.

Johnson, R.C., and Ely, B. (1977) Isolation of spontaneously derived mutants of *Caulobacter crescentus*. *Genetics* **86:** 25–32.

Jones, L.J., Carballido-Lopez, R., and Errington, J. (2001) Control of cell shape in bacteria: helical, actin-like filaments in *Bacillus subtilis*. *Cell* **104:** 913–922.

Kahan, F.M., Kahan, J.S., Cassidy, P.J., and Kropp, H. (1974) The mechanism of action of fosfomycin (phosphonomycin). *Ann NY Acad Sci* **235:** 364–386.

Kelly, A.J., Sackett, M.J., Din, N., Quardokus, E., and Brun, Y.V. (1998) Cell cycle-dependent transcriptional and proteolytic regulation of FtsZ in *Caulobacter*. *Genes Dev* **12:** 880–893.

Kruse, T., Moller-Jensen, J., Lobner-Olesen, A., and Gerdes, K. (2003) Dysfunctional MreB inhibits chromosome segregation in *Escherichia coli*. *EMBO J* **22:** 5283–5292.

Kruse, T., Bork-Jensen, J., and Gerdes, K. (2005) The morphogenetic MreBCD proteins of *Escherichia coli* form an essential membrane-bound complex. *Mol Microbiol* **55:** 78–89.

Lam, H., Schofield, W.B., and Jacobs-Wagner, C. (2006) A landmark protein essential for establishing and perpetuating the polarity of a bacterial cell. *Cell* **124:** 1011–1023.

Markiewicz, Z., Glauner, B., and Schwarz, U. (1983) Murein structure and lack of DD- and LD-carboxypeptidase activities in *Caulobacter crescentus*. *J Bacteriol* **156:** 649–655.

Mengin-Lecreulx, D., Texier, L., Rousseau, M., and van Heijenoort, J. (1991) The murG gene of *Escherichia coli* codes for the UDP-N-acetylglucosamine: N-acetylmuramyl-(pentapeptide) pyrophosphoryl-undecaprenol N-acetylglucosamine transferase involved in the membrane steps of peptidoglycan synthesis. *J Bacteriol* **173:** 4625–4636.

Mobley, H.L., Koch, A.L., Doyle, R.J., and Streips, U.N. (1984) Insertion and fate of the cell wall in *Bacillus subtilis*. *J Bacteriol* **158:** 169–179.

de Pedro, M.A., Quintela, J.C., Höltje, J.V., and Schwarz, H. (1997) Murein segregation in *Escherichia coli*. *J Bacteriol* **179:** 2823–2834.

de Pedro, M.A., Young, K.D., Holtje, J.V., and Schwarz, H. (2003) Branching of *Escherichia coli* cells arises from multiple sites of inert peptidoglycan. *J Bacteriol* **185:** 1147–1152.

Pinho, M.G., and Errington, J. (2003) Dispersed mode of *Staphylococcus aureus* cell wall synthesis in the absence of the division machinery. *Mol Microbiol* **50:** 871–881.

Poindexter, J.S., and Hagenzieker, J.G. (1981) Constriction and septation during cell division in caulobacters. *Can J Microbiol* **27:** 704–719.

Poindexter, J.S., and Hagenzieker, J.G. (1982) Novel peptidoglycans in *Caulobacter* and *Asticcacaulis* spp. *J Bacteriol* **150:** 332–347.

Rothfield, L. (2003) New insights into the developmental history of the bacterial cell division site. *J Bacteriol* **185:** 1125–1127.

Schmidt, J.M., and Stanier, R.Y. (1966) The development of cellular stalks in bacteria. *J Cell Biol* **28:** 423–436.

Shih, Y.L., and Rothfield, L. (2006) The bacterial cytoskeleton. *Microbiol Mol Biol Rev* **70:** 729–754.

Shih, Y.L., Kawagishi, I., and Rothfield, L. (2005) The MreB and Min cytoskeletal-like systems play independent roles in prokaryotic polar differentiation. *Mol Microbiol* **58:** 917–928.

Slovak, P.M., Wadhams, G.H., and Armitage, J.P. (2005) Localization of MreB in *Rhodobacter sphaeroides* under conditions causing changes in cell shape and membrane structure. *J Bacteriol* **187:** 54–64.

Slovak, P.M., Porter, S.L., and Armitage, J.P. (2006) Differential localization of Mre proteins with PBP2 in *Rhodobacter sphaeroides*. *J Bacteriol* **188:** 1691–1700.

Soufo, H.J., and Graumann, P.L. (2003) Actin-like proteins MreB and Mbl from *Bacillus subtilis* are required for bipolar positioning of replication origins. *Curr Biol* **13:** 1916–1920.

Steed, P., and Murray, R.G. (1966) The cell wall and cell division of gram-negative bacteria. *Can J Microbiol* **12:** 263–270.

Stephens, C., Mohr, C., Boyd, C., Maddock, J., Gober, J., and Shapiro, L. (1997) Identification of the *fliI* and *fliJ* components of the *Caulobacter* flagellar type III protein secretion system. *J Bacteriol* **179:** 5355–5365.

Taschner, P.E., Ypenburg, N., Spratt, B.G., and Woldringh, C.L. (1988) An amino acid substitution in penicillin-binding protein 3 creates pointed polar caps in *Escherichia coli*. *J Bacteriol* **170:** 4828–4837.

Terrana, B., and Newton, A. (1975) Pattern of unequal cell division and development in *Caulobacter crescentus*. *Dev Biol* **44:** 380–385.

Thanbichler, M., and Shapiro, L. (2006) MipZ, a spatial regulator coordinating chromosome segregation with cell division in *Caulobacter*. *Cell* **126:** 147–162.
Tiyanont, K., Doan, T., Lazarus, M.B., Fang, X., Rudner, D.Z., and Walker, S. (2006) Imaging peptidoglycan biosynthesis in *Bacillus subtilis* with fluorescent antibiotics. *Proc Natl Acad Sci USA* **103:** 11033–11038.
Umeda, A., and Amako, K. (1983) Growth of the surface of *Corynebacterium diphtheriae*. *Microbiol Immunol* **27:** 663–671.
Varma, A., and Young, K.D. (2004) FtsZ collaborates with penicillin binding proteins to generate bacterial cell shape in *Escherichia coli*. *J Bacteriol* **186:** 6768–6774.
Vollmer, W., and Höltje, J.V. (2001) Morphogenesis of *Escherichia coli*. *Curr Opin Microbiol* **4:** 625–633.
Wachi, M., Doi, M., Tamaki, S., Park, W., Nakajima-Iijima, S., and Matsuhashi, M. (1987) Mutant isolation and molecular cloning of *mre* genes, which determine cell shape, sensitivity to mecillinam, and amount of penicillin-binding proteins in *Escherichia coli*. *J Bacteriol* **169:** 4935–4940.
Wang, Y., Jones, B.D., and Brun, Y.V. (2001) A set of *ftsZ* mutants blocked at different stages of cell division in *Caulobacter*. *Mol Microbiol* **40:** 347–360.
Woldringh, C.L., Huls, P., Pas, E., Brakenhoff, G.J., and Nanninga, N. (1987) Topography of peptidoglycan synthesis during elongation and polar cap formation in a cell division mutant of *Escherichia coli* MC4100. *J Gen Microbiol* **133:** 575–586.
Young, K.D. (2006) The selective value of bacterial shape. *Microbiol Mol Biol Rev* **70:** 660–703.

Supplementary material

The following supplementary material is available for this article:

Methods. Construction methods for strains and plasmids.
Figure S1. Peptidoglycan elongation occurs near midcell in *C. crescentus*.
Figure S2. Localization pattern of MurG–mGFP.
Figure S3. Localization of GFP–MreB and FtsZ–mCherry in the presence of A22.
Figure S4. Cell morphology of CB15N $mreB_{Q26P}$ cells.
Figure S5. The effect of fosfomycin on cell growth.
Table S1. Strains and plasmids.
Movie S1. Time-lapse movie showing the relative localization of MurG and FtsZ during the cell cycle.
Movie S2. Time-lapse movie showing the relative localization of MreB and FtsZ during the cell cycle.
Movie S3. Time-lapse movie of MurG localization under conditions of FtsZ depletion.
Movie S4. Time-lapse movie of $MreB_{Q26P}$ localization in the $mreB_{Q26P}$ mutant background.
Movie S5. Time-lapse movie of MurG and FtsZ localization in a $mreB_{Q26P}$ mutant background.

This material is available as part of the online article from:
http://www.blackwell-synergy.com/doi/abs/10.1111/j.1365-2958.2007.05720.x
(This link will take you to the article abstract).

Please note: Blackwell Publishing is not responsible for the content or functionality of any supplementary materials supplied by the authors. Any queries (other than missing material) should be directed to the corresponding author for the article.

